Open Questions in Large-Scale Structure

J. Frieman

- What is the Correct Framework?
  - Gravity? Something else?
- What is the Origin of Perturbations?
  - Inflation?
  - Topological Defects?
  - Something else?

Gaussian or non-Gaussian?

What is the shape of the large-scale power spectrum?

- What is the Dark Matter and How Much?
  - Cold?
  - Hot?
  - Cold plus Hot?
  - Warm?
  - Tepid?
  - Frozen?
  - MACHOs?
  - Λ?
  - Ω?
  - something else?
- How Do Galaxies Form?
  - Bias: How are galaxies related to the mass distribution?
- How Does the Pattern of Large-Scale Clustering Arise?

Structure Formation in Brief

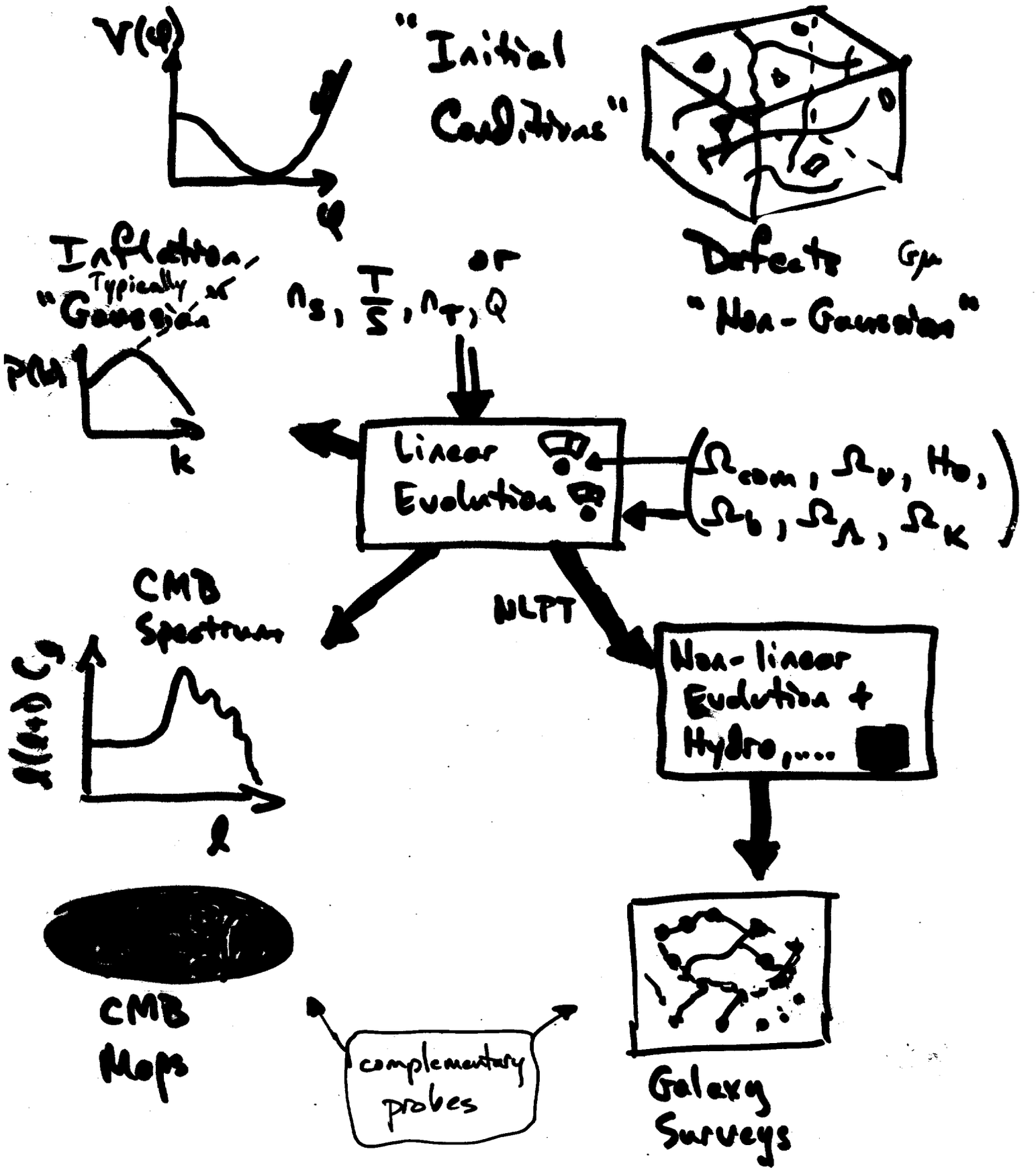

Sloan Digital Sky Survey (SDSS)

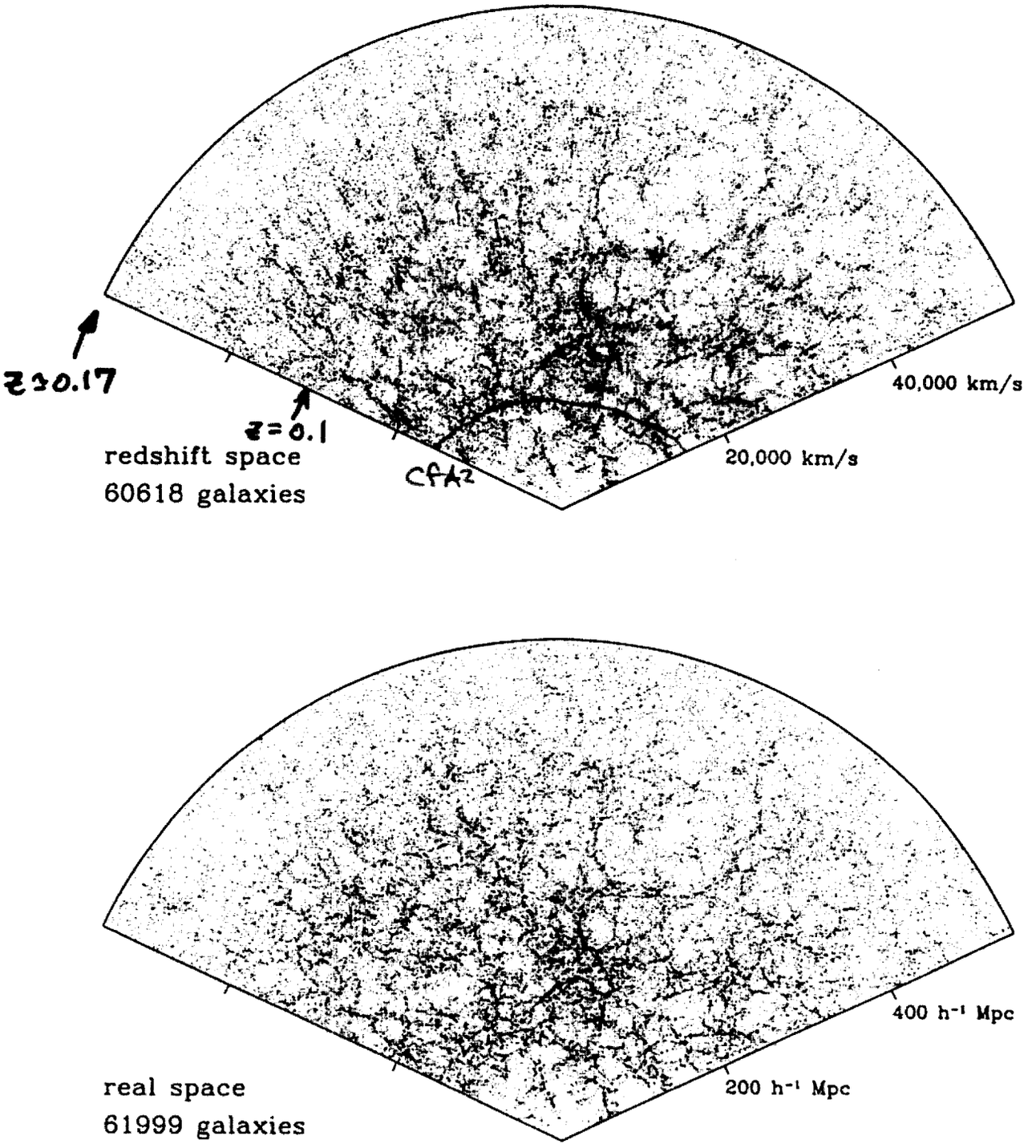

Fig. 1.— Galaxy distribution in a 6° slice along the survey equator. in redshift space (upper plot) and real space (lower plot).

Weinberg, Park, Gott

Galaxy Power Spectrum

Density Field: $\rho(\vec{x},t) = \bar{\rho}(t)[1+\delta(\vec{x},t)]$

$$\delta_{\vec{k}} = \int d^3x\, e^{-i\vec{k}\cdot\vec{x}}\delta(\vec{x},t) \qquad \langle \delta_{\vec{k}}\delta^*_{\vec{k}'}\rangle = P(k)\,\delta^3(\vec{k}+\vec{k}')$$

Fourier Transform

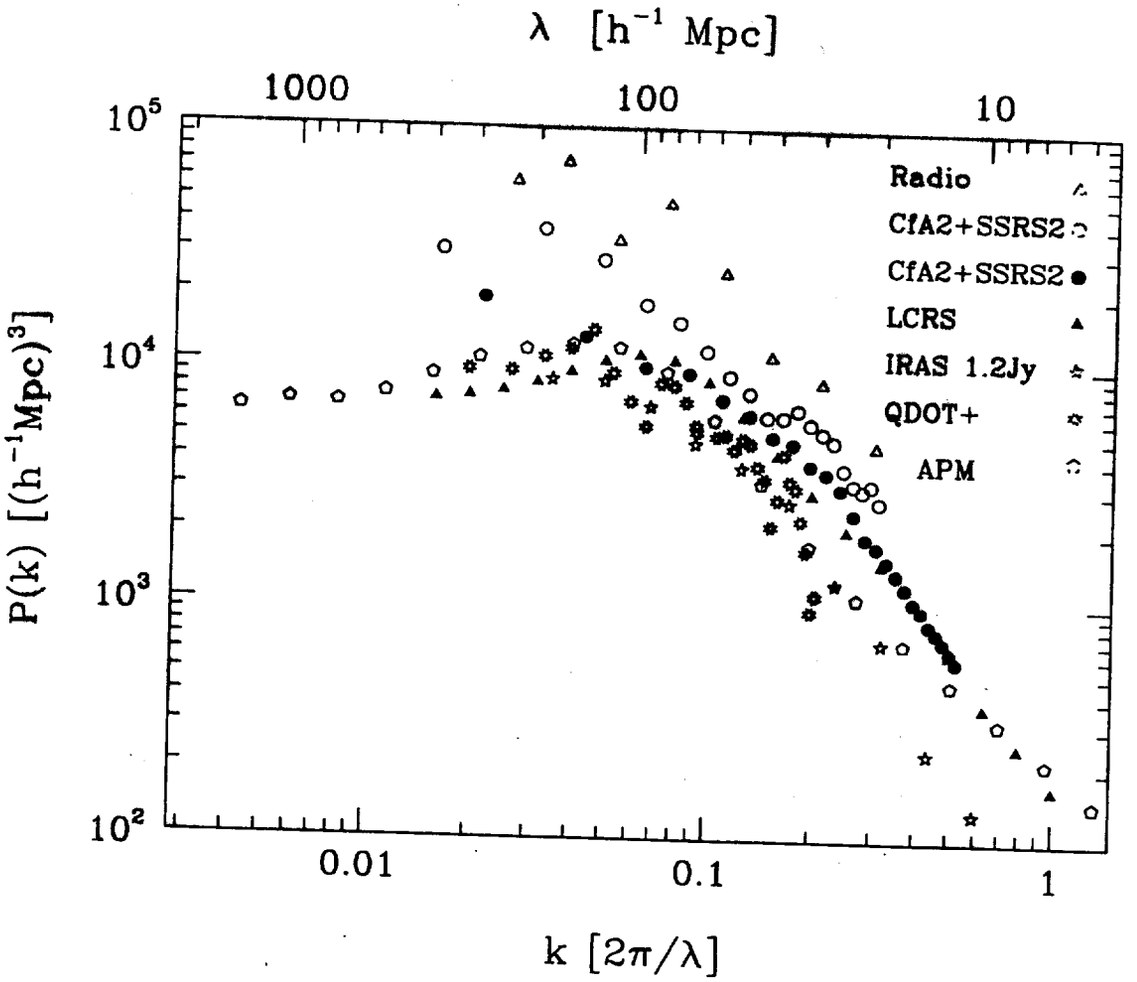

Fig. 1a.— Estimates of the redshift-space power spectrum from a variety of redshift surveys, and an estimate of the real-space power spectrum inferred from angular correlations (APM).

Vogeley

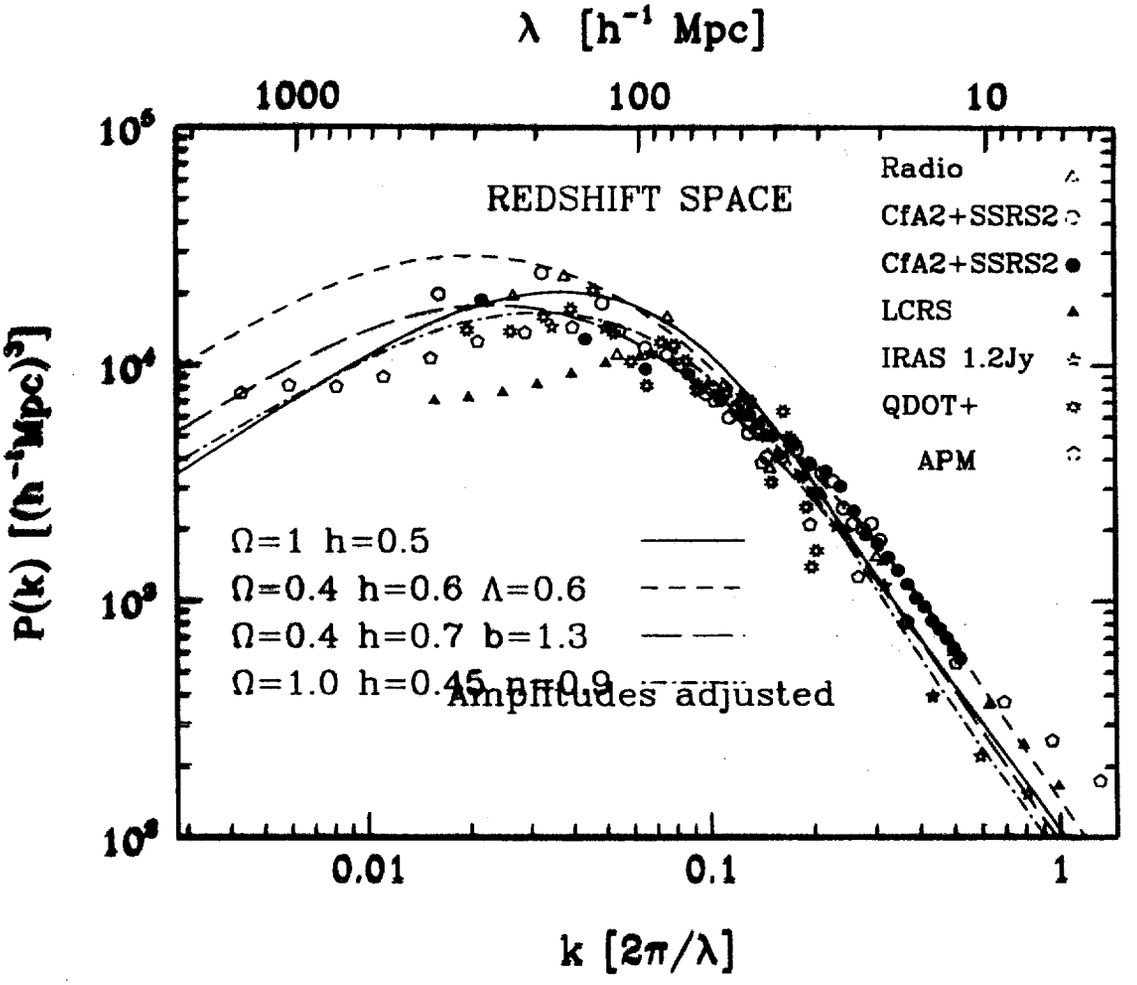

Fig. 2b. — Nonlinear redshift-space power spectra from Figure 1a [redacted] models. Amplitudes adjusted to allow comparison of power spectrum shapes. CfA2+SSRS2-101 and LCRS were not adjusted.

Broadhurst, et al.

Deep pencil beams:

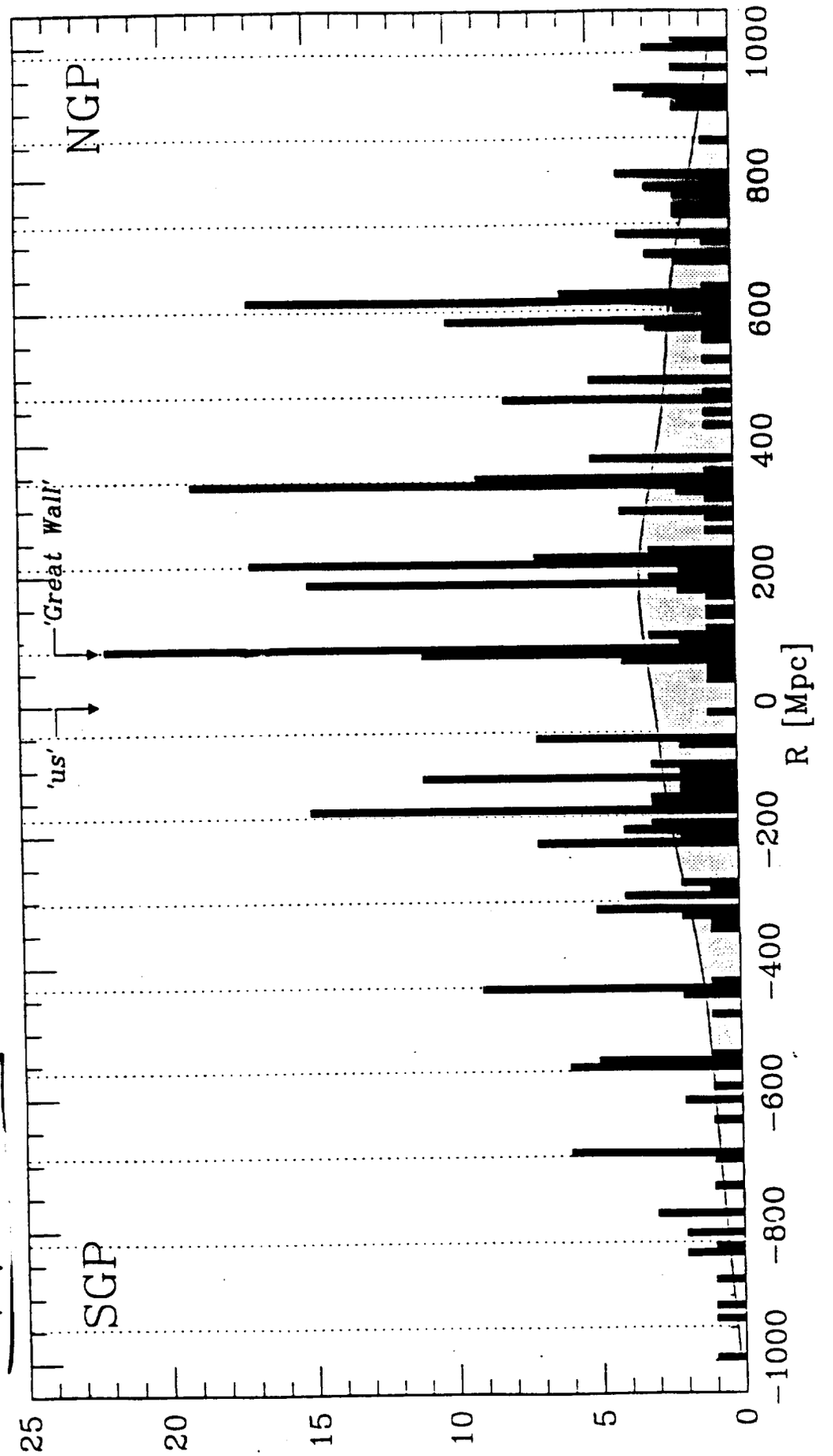

Additional fields:
periodicity less significant, but spikes remain (even when fields combined)

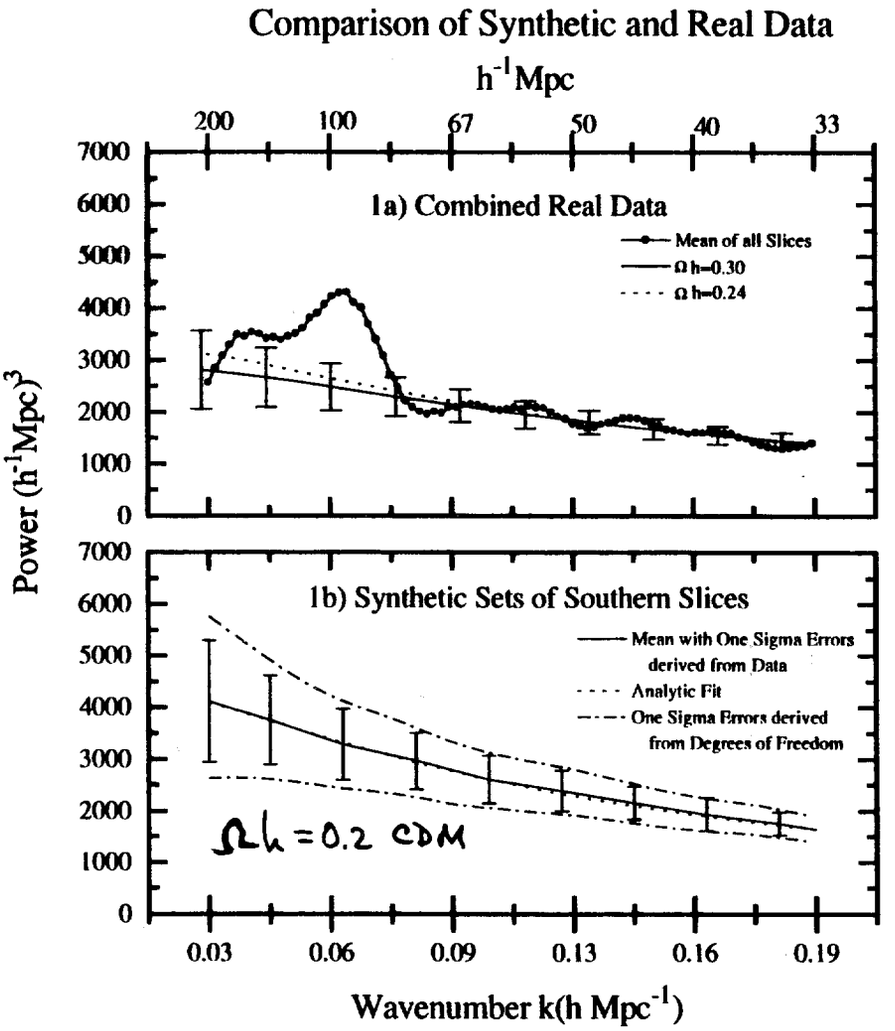

Las Campanas Redshift Survey : 2D P(k)

Landy, etal.

APM Power Spectrum

$n = d\ln P(k)/d\ln k$ slope

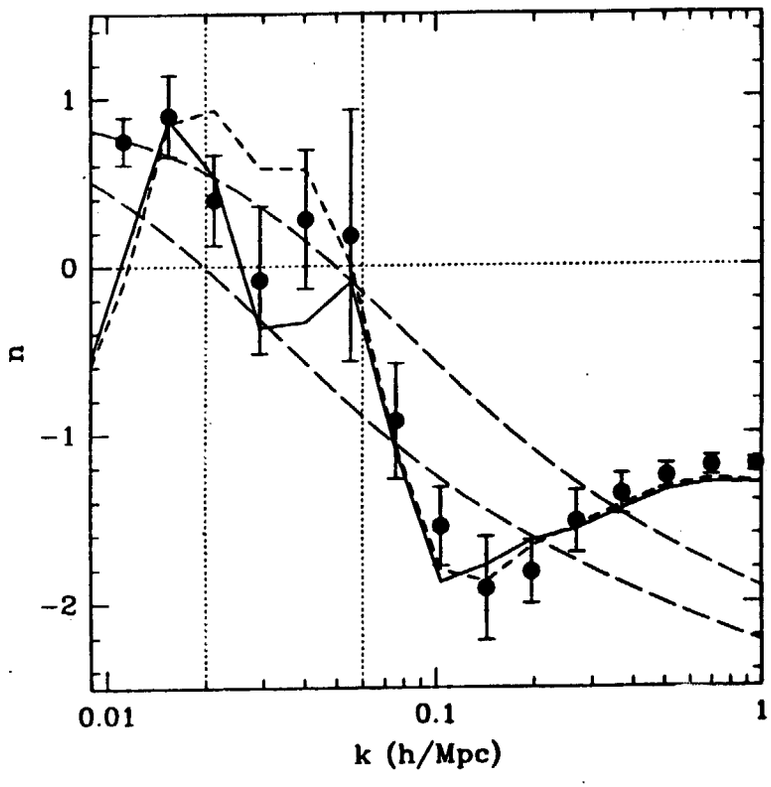

Figure 13. The local slope of the power spectrum estimated from the APM catalogue. Symbols with errorbars correspond to the slope estimated in 4 individual disjoint zones (subsamples). The continuous line is from an inversion of the angular correlation function measured from the full APM map. The short dashed line corresponds to the inversion after subtracting 10^{-3} from the angular correlation function in the full APM map. The two long-dashed lines correspond to linear CDM models with $\Omega h = 0.5$ (top) and $\Omega h = 0.2$ (botom).

Gaztañaga + Baugh

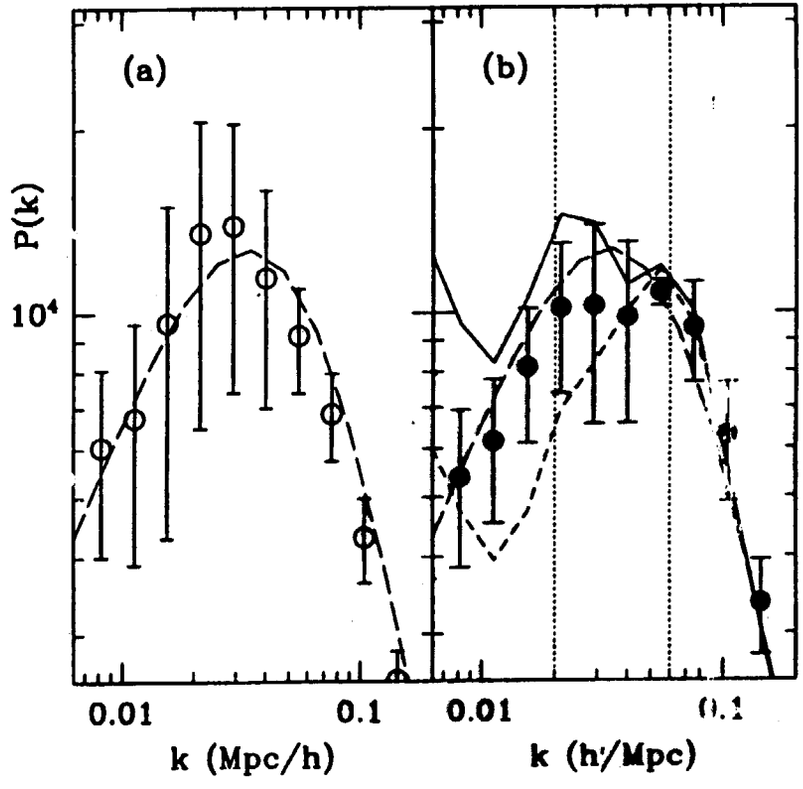

Figure 14. Comparison of the recovered $P(k)$ (points with errorbars), from the angular catalogues with the linear APM model (long-dashed line). Panel (a) corresponds to a mock APM catalogue [APM2(a)]. Panel (b) shows the estimated APM $P(k)$ from measurements in the real galaxy catalogue. In both cases the points and errorbars correspond to the mean and variance in 4 individual disjoint zones (subsamples). The continuous line in panel (b) corresponds to the inversion result obtained using the angular correlation function measured from the full APM map. The short-dashed line corresponds to the inversion result after subtracting an offset of 10^{-3} from $w(\theta)$.

SLOAN DIGITAL SKY SURVEY

Univ. of Chicago
Fermi National Accelerator Laboratory
Princeton U., Institute for Advanced Study
Johns Hopkins U., U. of Washington, Naval Observatory
Japan Participation Group

GOAL: MAP THE UNIVERSE IN 3-DIMENSIONS OVER LARGE VOLUME

OUTPUT:

- 100 MILLION 5-color IMAGES – Photometric Survey
- 1 MILLION GALAXY REDSHIFTS
- 10^5 QSO REDSHIFTS
- 10^5 BRGs

} – Spectroscopic Survey

- VARIABLE OBJECTS

SDSS

TECHNOLOGICAL DEVELOPMENTS:

- 2.5 M DEDICATED TELESCOPE
  - wide field (3° x 3°) — 10,000 □° Northern Survey
  - Apache Pt. Observatory (next to ARC 3.5M)

- VERY LARGE CCD CAMERA

3540Å u' g' r' i' z' 9250Å ← Star/Galaxy/QSO separation + photometric z's

  - 30 2048 x 2048 CHIPS 0.4" / pixel
  - Drift-scan mode

- r' ≤ 23.1 w/ S/N > 5 for point sources

Time: ~20% imaging
~80% spectroscopy
- 5+ yrs. duration

- MULTI-FIBER SPECTROSCOPY
  - 2 DOUBLE FIBER-FED SPECTROGRAPHS
  - 640 FIBERS ON THE SKY (PLUG PLATES) pre-drilled

- Galaxies r' ≤ 18.1 - QSO's g' ≤ 19.7

- DATA ACQUISITION/PROCESSING
  - Terabytes of data
  - Turn around imaging ⇒ spectroscopic target selection

- South: repeated scans ⇒ 2 mag deeper than Northern Survey
  225 □°

APACHE POINT OBSERVATORY
NEW MEXICO

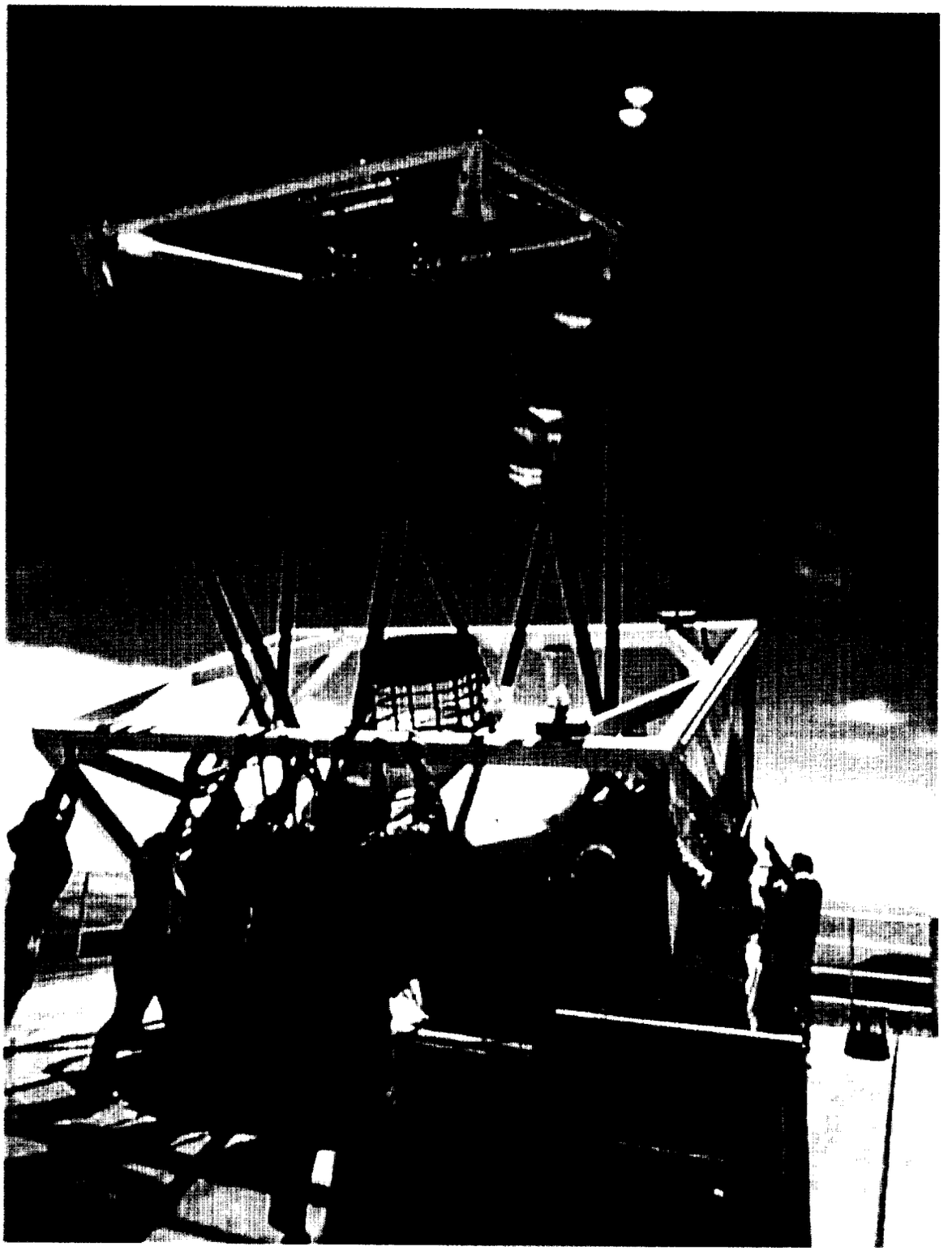

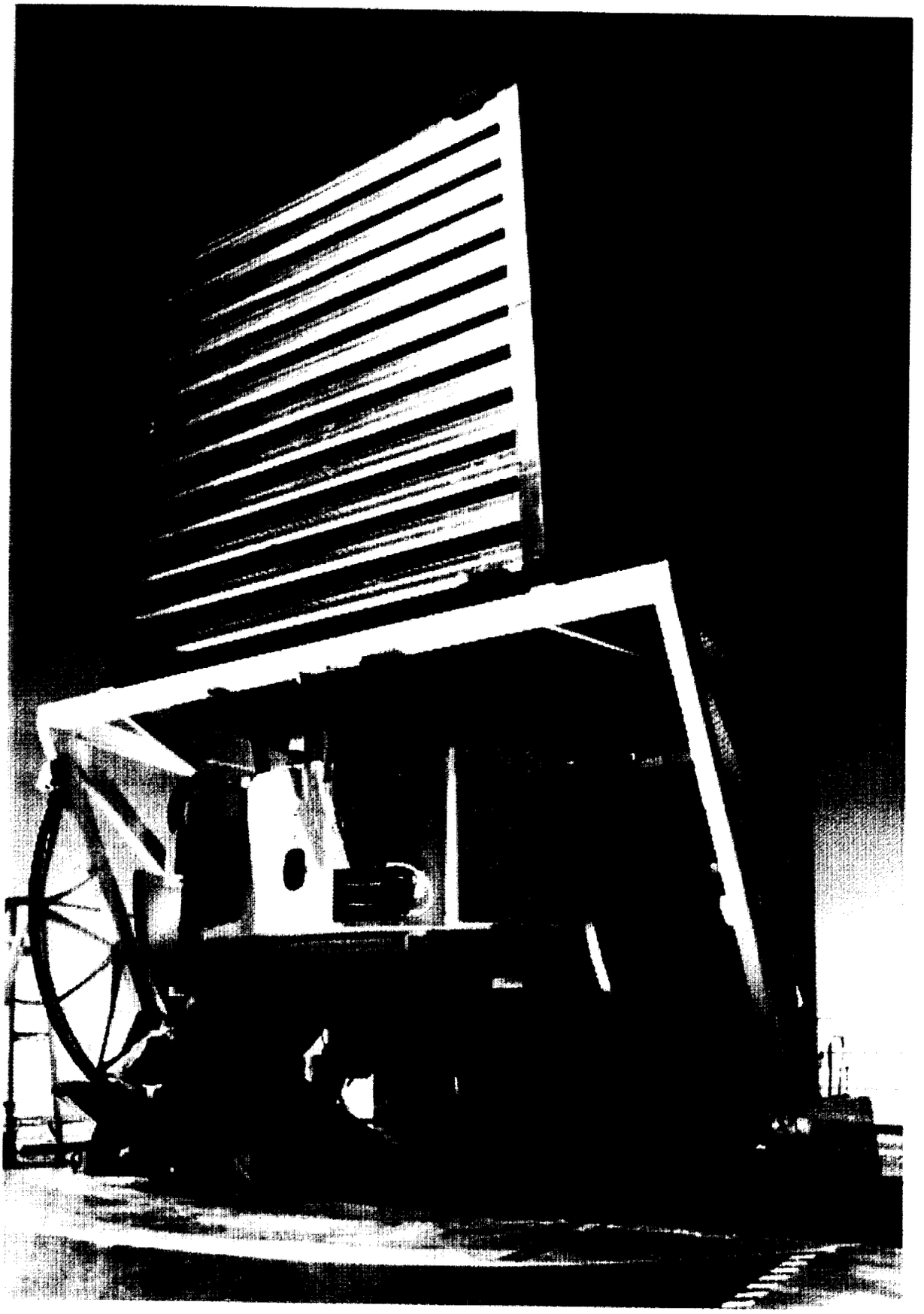

Figure 13. "Assembly" drawing showing the six photometric dewars and the two astrometric ones as attached to the distortion corrector. The outlines of all the CCDs are shown except the focus monitor, which is in the trailing (lower) astrometric dewar. The design of the astrometric dewars is in a very preliminary state (the CCD design itself was only very recently defined) but the photometric ones are in the prototype stage (see Figures 15, 16, and 17).

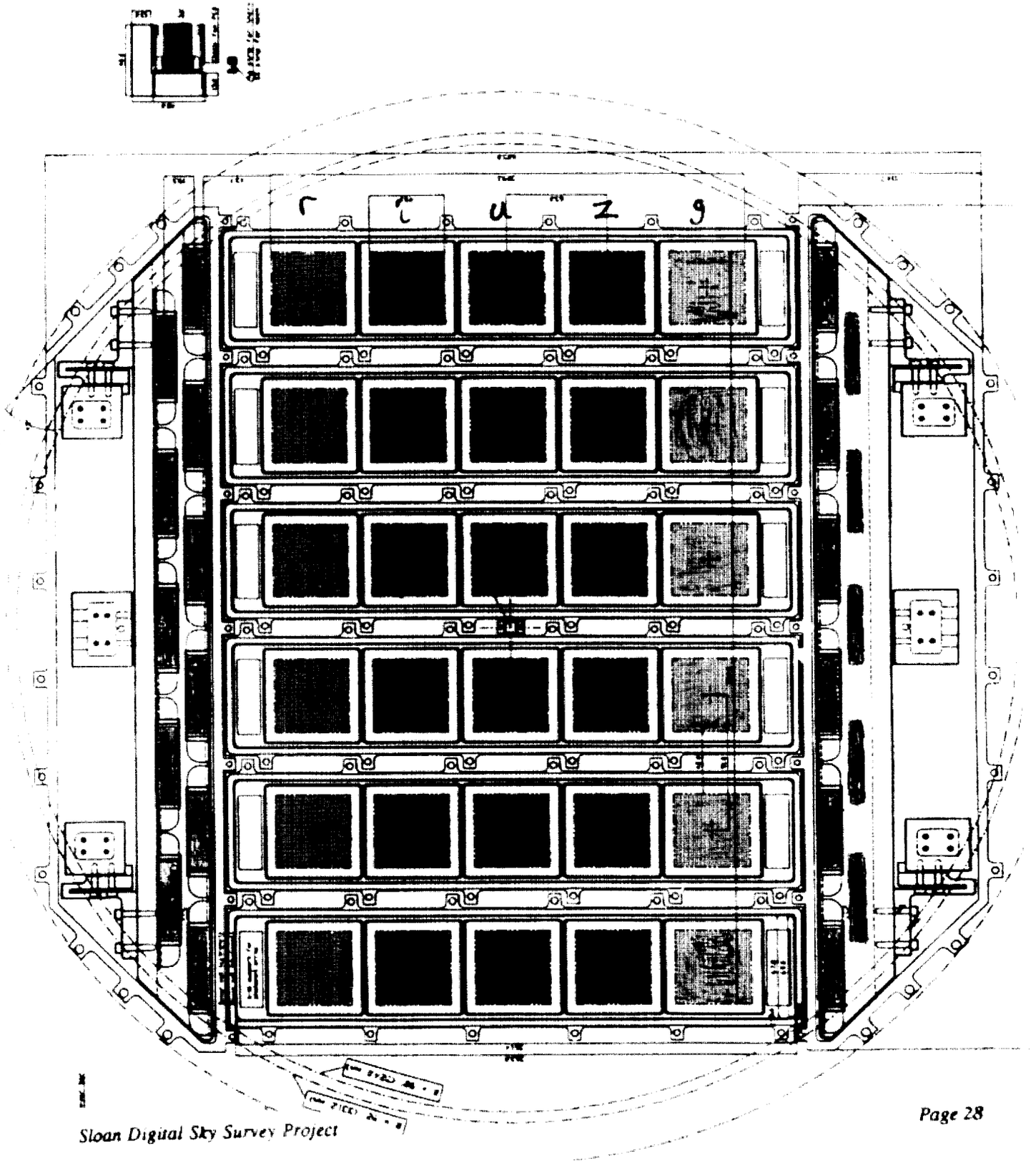

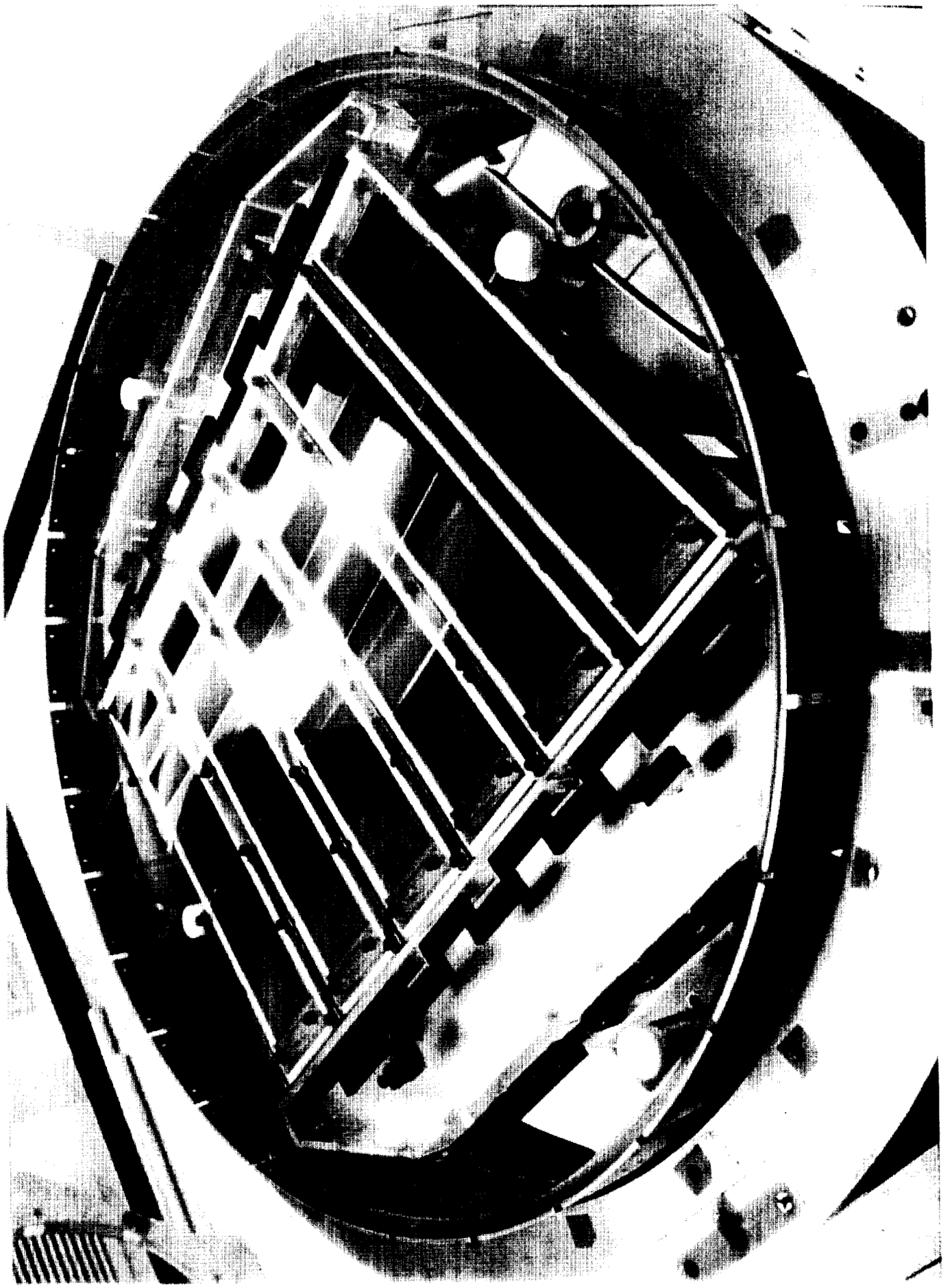

photometric data may lead to improvements in the distance indicators (Connolly 1993), or to completely new redshift-independent measures of distance.

Photometric Redshifts

While the SDSS galaxy redshift survey will be complete to $r' \approx 18.1$, the photometric data extend 5 magnitudes deeper for the Northern sample and 7 magnitudes deeper for the Southern strip. We can substantially increase the power of the SDSS by deriving approximate galaxy redshifts from the broad-band colors. Photometric redshifts are accurate enough for basic measures of the evolution of the galaxy population and of galaxy clustering. Deriving approximate redshifts to the limit of the photometric survey will increase the number of objects available for study of the spatial distribution of galaxies from 10^6 to 5×10^7.

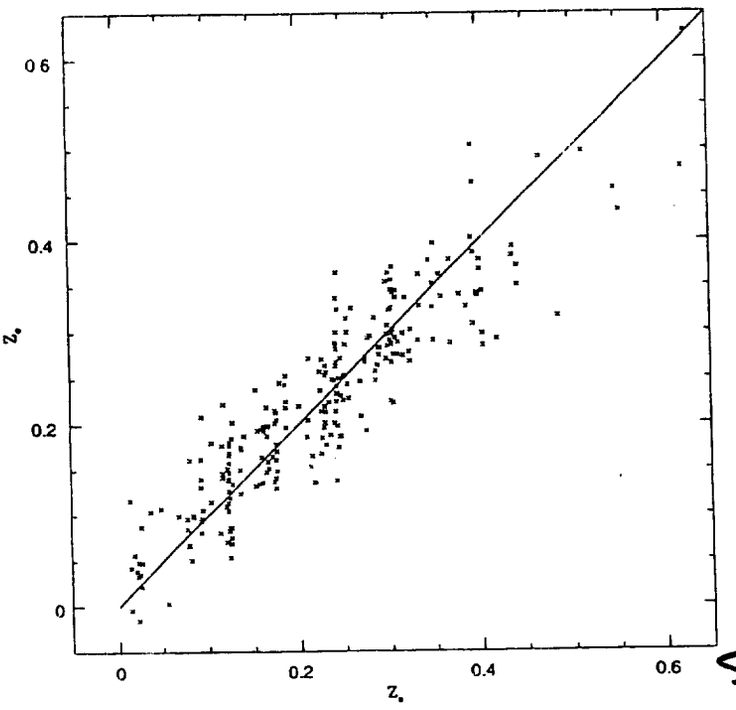

Figure 3.1.11 Estimating redshifts from photometry. The figure shows the estimated redshift *vs.* the spectroscopic redshift for the Koo and Kron UJFN photographic data, to $B_J = 22.5$. The formal dispersion is $\Delta z = 0.047$, largely dominated by photometric errors. The underestimate of galaxy redshifts at faint magnitudes is due to Malmquist bias. From Connolly *et al.* (1995).

Deep multi–color photographic data in the selected areas SA57 and SA68 (*cf.* Koo and Kron 1992) have shown that the distribution of galaxies in the four-color space U, B_J, R_F, I_N is almost planar (Connolly *et al.* 1995). In this plane, lines of constant redshift and lines that trace the luminosity evolution of galaxy spectral types are almost orthogonal. The dispersion in the color-redshift relation is $\Delta z = 0.047$ to $B_J = 22.5$ (Figure 3.1.11), where the scatter is already dominated by photometric errors. We have modeled the relation given the signal-to-noise ratio of the SDSS and find that the dispersion reduces to $\Delta z = 0.02$ for $z < 1$, especially for the reddest galaxies (cf. Section 3.2.2). The photometric survey of the

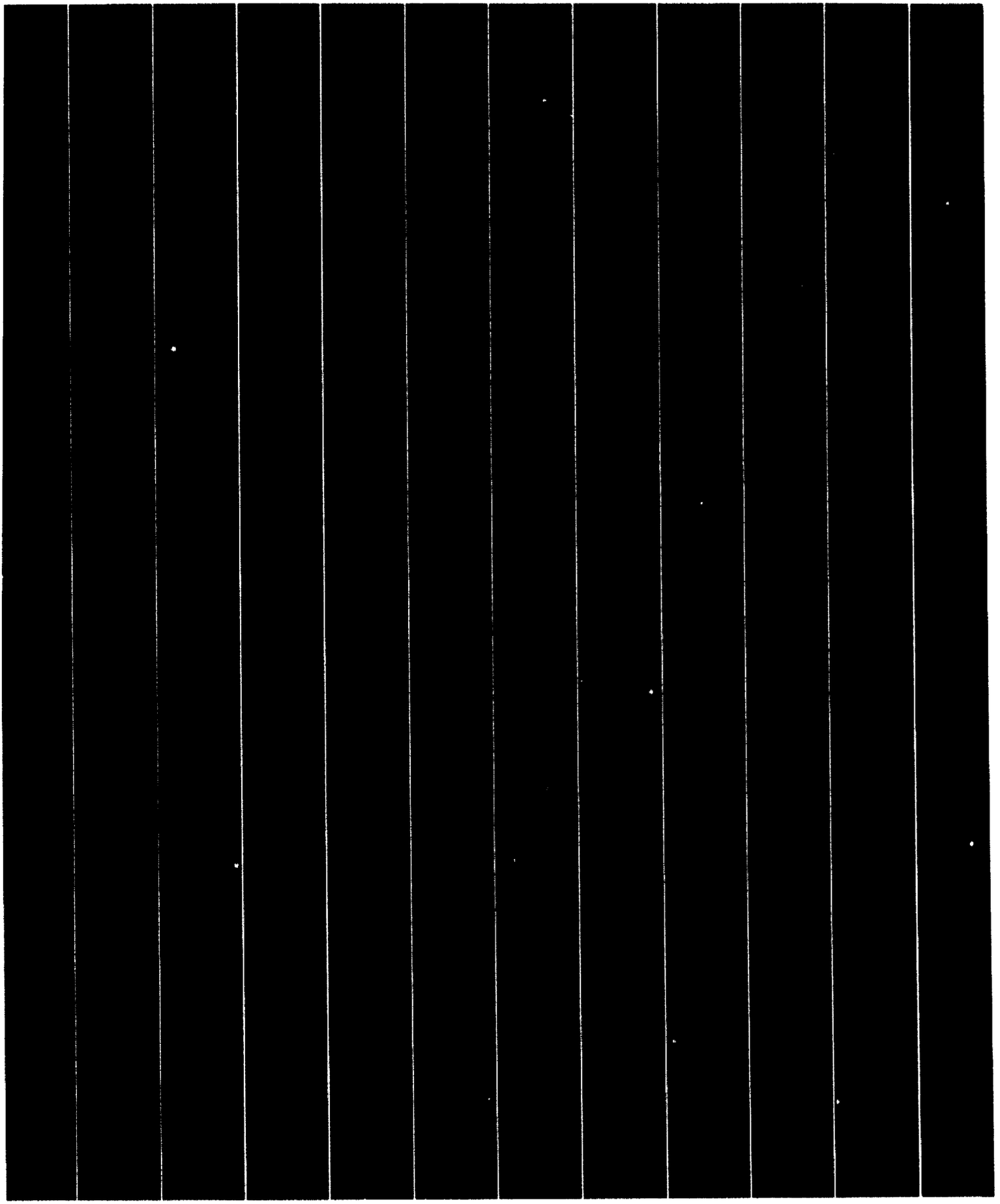

2.5°

Sloan Digital Sky Survey

first light

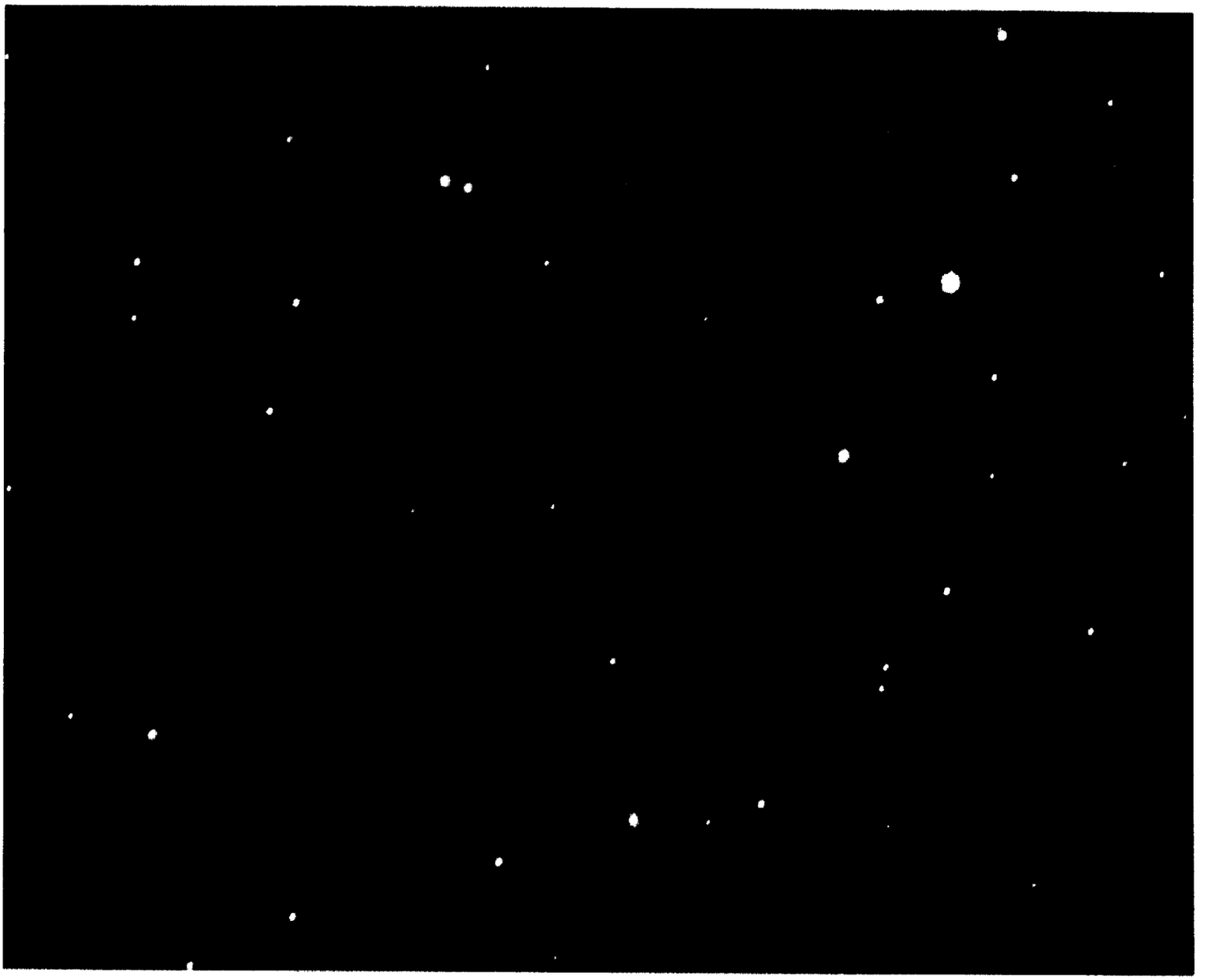

Constellation Serpens

http://www.sdss.org

SDSS First Light

NGC 6070

$V_{rec} \approx 2000$ km/sec

http://www.sdss.org

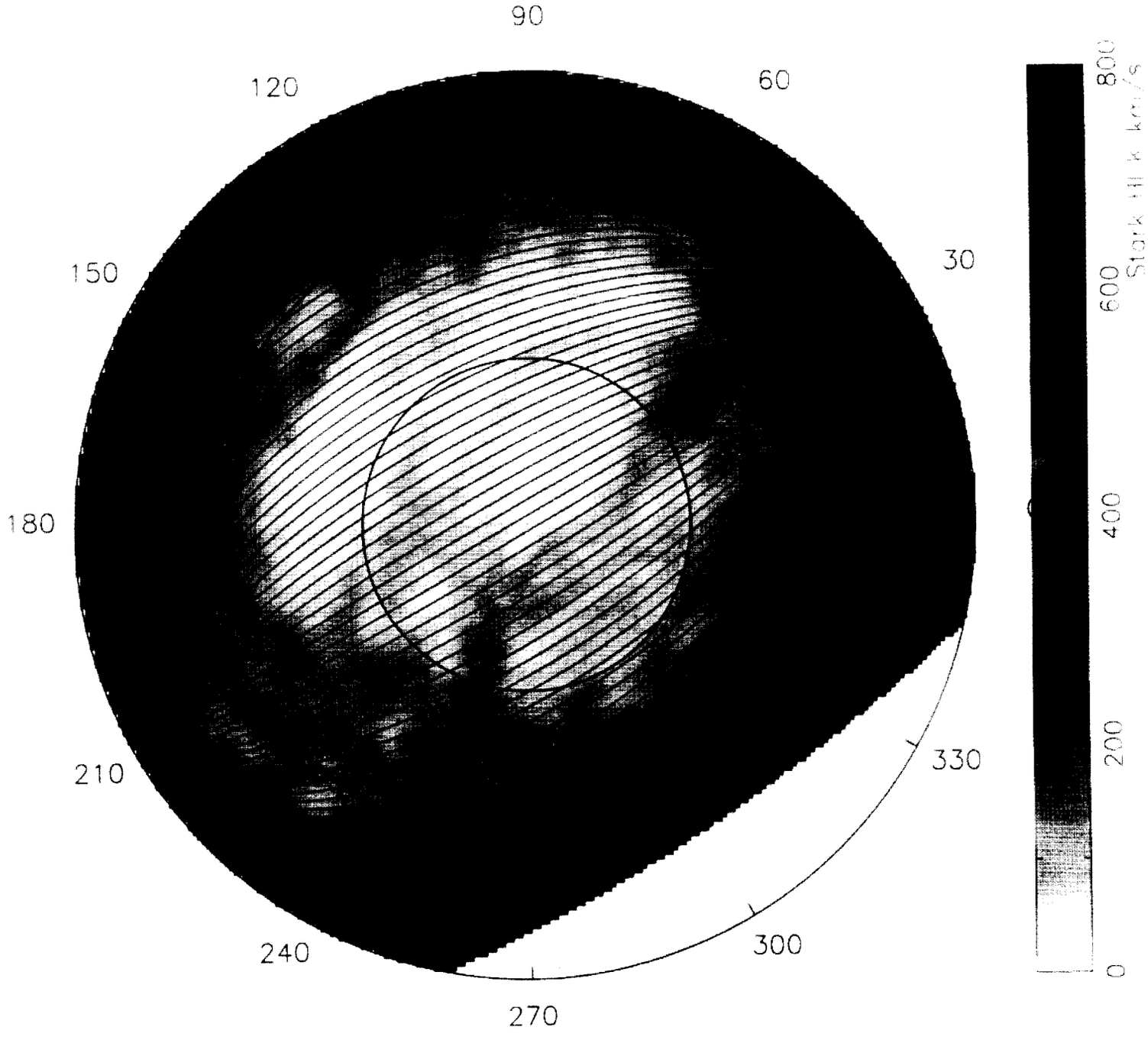
90
120
60
150
30
180
210
330
240
300
270
800
600
400
200
0

SDSS Power Spectrum Determination

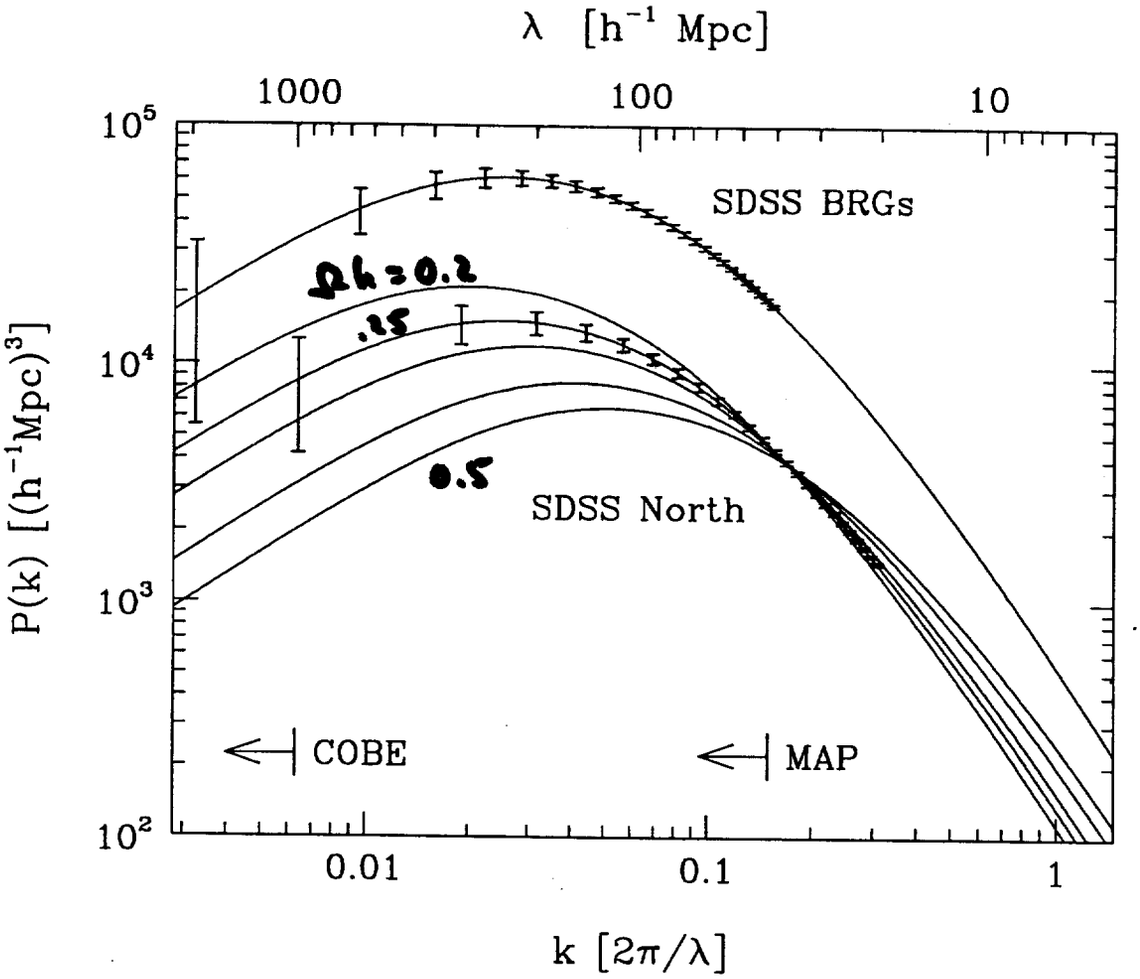

Fig. 3.— Predicted uncertainties in the power spectrum estimated from a volume-limited ($R_{max} = 500h^{-1}$ Mpc) sample of SDSS North and for the Bright Red Galaxy sample (upper set of error bars). These errors assume that the true power spectrum is that of an $\Omega h = 0.25$ CDM model and that the BRGs are more clustered than normal galaxies. Plotted for comparison to the SDSS North errors are CDM power spectra (normalized to $\sigma_8 = 1$) for a range of Ωh from 0.2 (uppermost curve) to 0.5 (lowest curve) and indications of the range of comoving scales probed by the COBE and MAP CMB anisotropy experiments.

Vogeley

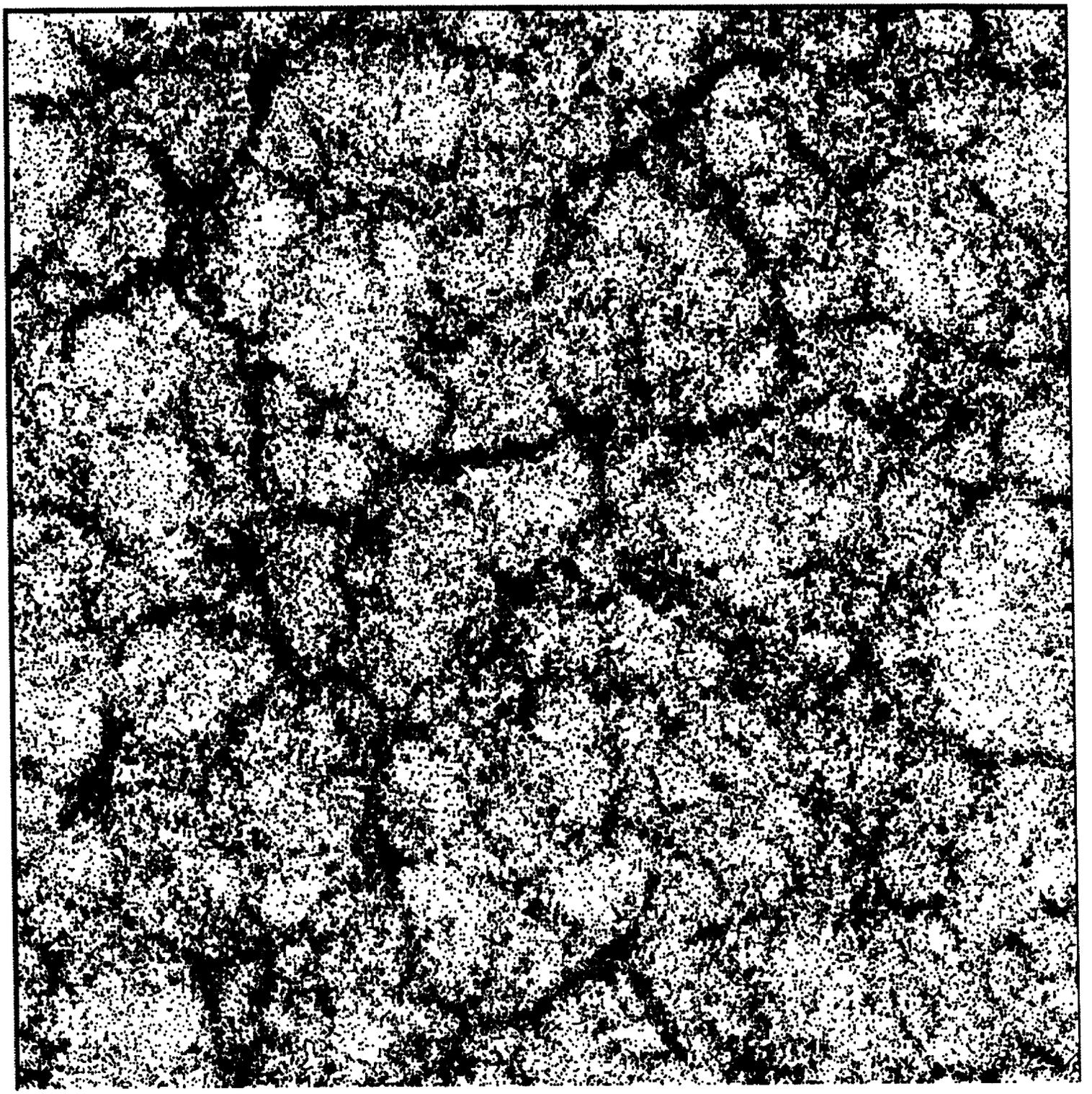

Very Large Mock Catalogs for SDSS

stebbins

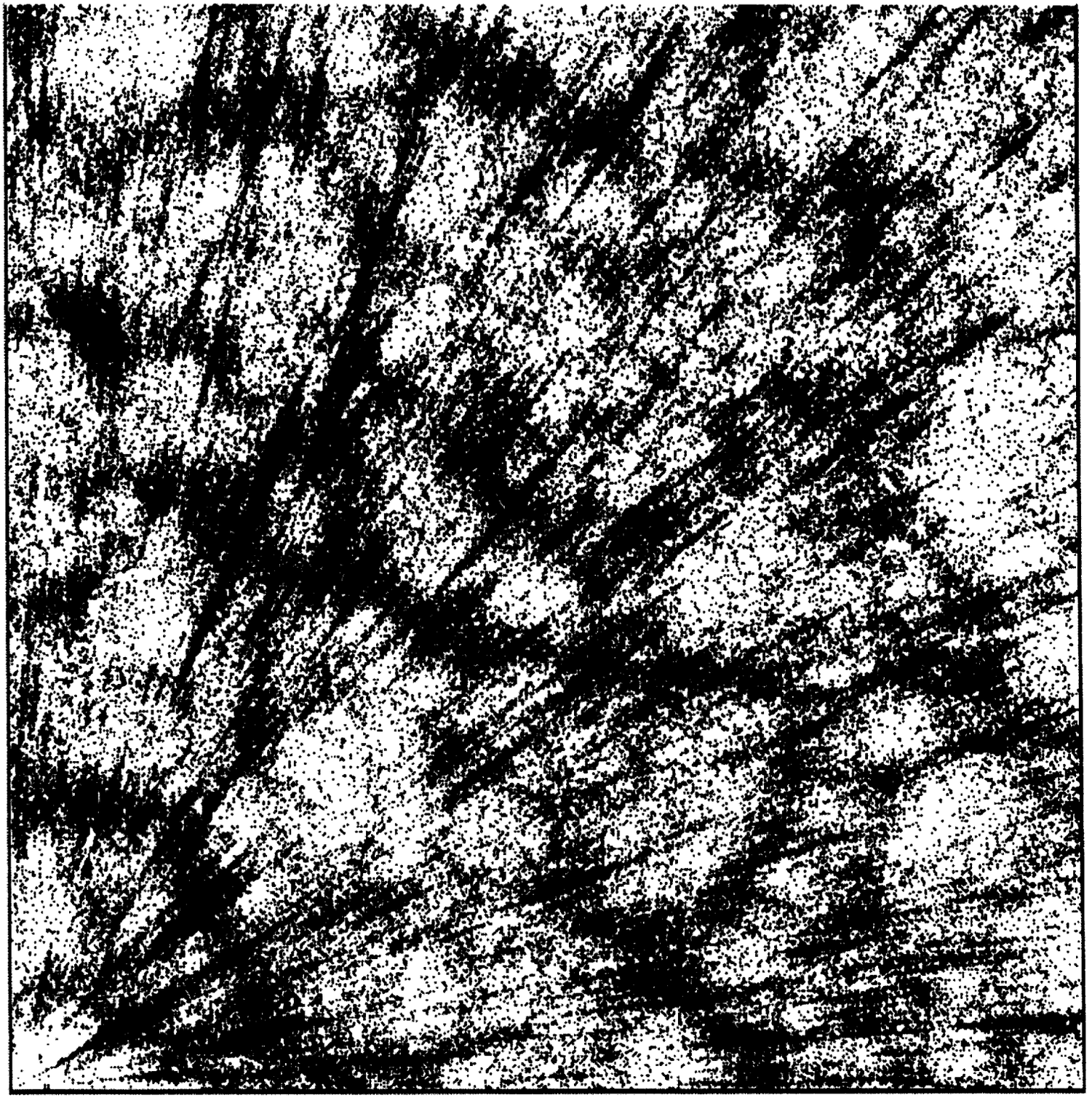

Redshift Catalog

Redshift Distortions and Ω

- large scales: linear flow + turn-around
- small scales: finger of God due to internal velocity dispersion

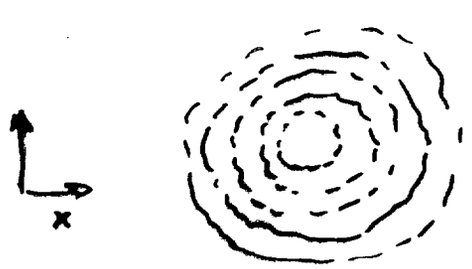

Real Space
density contours

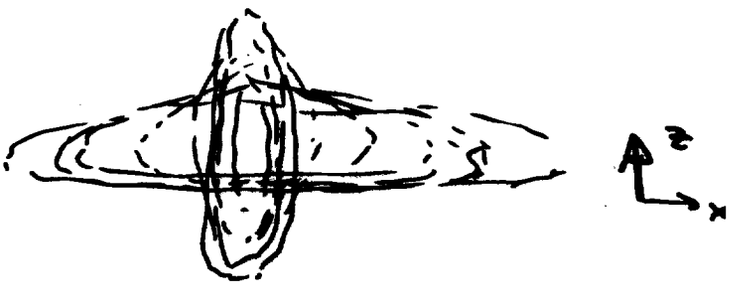

Redshift space

$$cz = H_0 r + \vec{v}_{pec} \cdot \hat{r}$$

- Clustering in redshift surveys is distorted by peculiar velocities. (cf. CFA)
- Use anisotropy of redshift-space clustering to measure $\boxed{\beta = \Omega_m^{0.6}/b}$

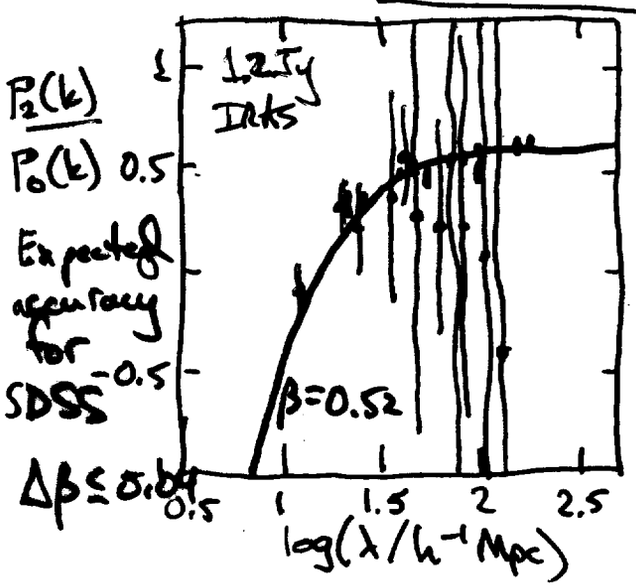

$$\delta(\vec{k}) = \int d^3x\, e^{i\vec{k}\cdot\vec{x}}\, \delta_{gal}(\vec{x})$$

$$P(\vec{k}) = \langle |\delta(\vec{k})|^2 \rangle$$

Kaiser

$$P_R(k,\mu) \simeq P(k)(1+\beta\mu^2)^2 \exp(-k^2\sigma_v^2\mu^2)$$

$$\mu = \cos(\vec{k}\cdot\vec{r})$$

$$P_R(k,\mu) = \sum_l P_l(k) L_l(\mu)$$

Cole, Fisher, Weinberg

$k \to 0$

$$\frac{P_2}{P_0} \simeq \frac{\frac{4}{3}\beta + \frac{4}{7}\beta^2}{1 + \frac{2}{5}\beta + \frac{1}{5}\beta^2}$$

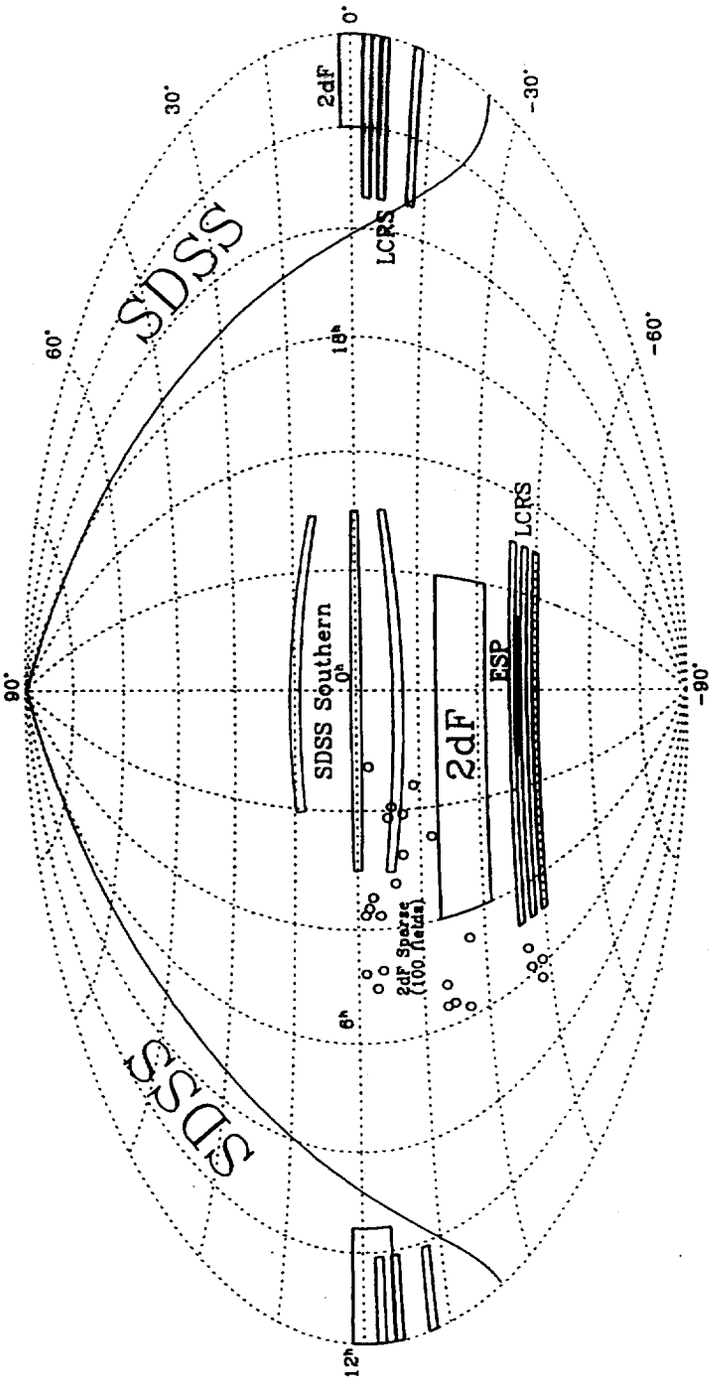

Figure A.1 Sky coverage of various redshift surveys (Strauss 1996)

The 3-point Galaxy Correlation Function in Wide-Field Surveys

Probes:
- bias
- non-Gaussianity
- features in $P(k)$
- Ω
- non-linear evolution

- APM : $\xi_3(\theta_1, \theta_2, \theta_3)$ Angular 3-pt. fn. Gaztanaga
- Redshift-space Clustering: $P(k)$ and $B(k_1, k_2)$: theory Scoccimarro Couchman
- IRAS 1.2 Jy + QDOT : $B(k_1, k_2)$ Bispectrum results Feldman, Fry
- SDSS : $B(k_1, k_2)$ and Ω_B features Joffre
- Probing Non-Gaussianity : Isocurvature CDM Juszkiewicz

Statistical Observables

Multi-point Functions

$$\delta(\vec{r}) = (\rho(\vec{r}) - \bar{\rho})/\bar{\rho}$$

$$\boxed{\xi(\vec{r}_1, \ldots, \vec{r}_N) = \langle \delta(\vec{r}_1) \ldots \delta(\vec{r}_N) \rangle}$$ in real/redshift space

Fourier space: $\delta(\vec{k}) = \int d^3r \; \delta(\vec{r}) e^{i\vec{k}\cdot\vec{r}}$

$$\langle \delta(\vec{k}_1) \ldots \delta(\vec{k}_N) \rangle_c = P(\vec{k}_1, \ldots, \vec{k}_N) \delta_D(\vec{k}_1 + \cdots \vec{k}_N)$$

$N=2$: power spectrum
$N=3$: bispectrum ...

Connected $N>2$ functions zero for Gaussian (inflation)

Moments of Smoothed PDF (Counts-in-Cells)

Smoothed density field: $\delta_R(\vec{x}) = \int d^3r \; \delta(\vec{x}+\vec{r}) \, W(\vec{r})$

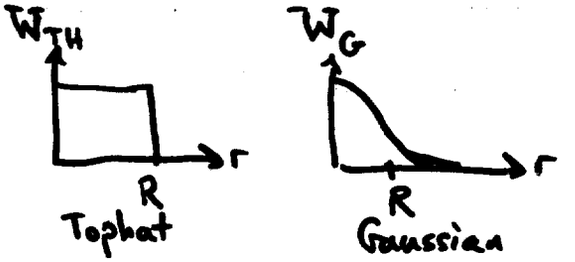

Probability Distn. Fn.

Moments: $\langle \delta_R^J \rangle_c = \int \mathcal{P}(\delta_R) \delta_R^J \, d\delta_R$

$$= \int d^3k_1 \cdots d^3k_J \langle \delta(\vec{k}_1) \cdots \delta(\vec{k}_J) \rangle_c \, \hat{W}(\vec{k}_1 R) \cdots \hat{W}(\vec{k}_J R)$$

$J=2$: variance $\langle \delta_R^2 \rangle \equiv \sigma_R^2$

Hierarchical Amplitudes:

$$\boxed{S_J(R) = \frac{\langle \delta_R^J \rangle_c}{\langle \delta_R^2 \rangle^{J-1}}}$$

Independent Probes of LSS

$J=3$: skewness
$J=4$: kurtosis
$J=5$: psoriasis
⋮

} vanish for Gaussian

Non-Linear Perturbation Theory

Fluid Dynamics (CDM before shell-crossing) $\rho(\vec{x},t) = \bar{\rho}(t)[1+\delta(\vec{x},t)]$

$\dot{} = \frac{\partial}{\partial \tau}$, $d\tau = dt/a$, $\mathcal{H} = \frac{1}{a}\frac{da}{d\tau}$, conformal time + comoving coords.

$$\dot{\delta} + \vec{\nabla}\cdot[(1+\delta)\vec{v}] = 0 \qquad \text{Continuity}$$

$$\dot{\vec{v}} + \mathcal{H}\vec{v} + (\vec{v}\cdot\vec{\nabla})\vec{v} = -\nabla\Phi \qquad \text{Momentum conservation}$$

$$\nabla^2\Phi = \tfrac{3}{2}\Omega\mathcal{H}^2\delta \qquad \text{Poisson}$$

- Assume $\vec{\nabla}\times\vec{v} = 0$ (preserved by evolution (before shell crossing)) and define $\theta = \vec{\nabla}\cdot\vec{v}$ ← Potential Flow

Momentum Space Non-linearity ⇒ Mode Coupling

$$\dot{\delta}(\vec{k}) + \theta(\vec{k}) = -\int\!\!\int d^3k_1 d^3k_2\, \delta_D(\vec{k}-\vec{k}_1-\vec{k}_2)\,\frac{\vec{k}\cdot\vec{k}_1}{k_1^2}\,\theta(\vec{k}_1)\delta(\vec{k}_2)$$

$$\dot{\theta}(\vec{k}) + \mathcal{H}\theta(\vec{k}) + \tfrac{3}{2}\Omega\mathcal{H}^2\delta(\vec{k}) = -\int\!\!\int d^3k_1 d^3k_2\, \delta_D(\vec{k}-\vec{k}_1-\vec{k}_2)\,\frac{k^2(\vec{k}_1\cdot\vec{k}_2)}{2k_1^2k_2^2}\,\theta(\vec{k}_1)\theta(\vec{k}_2)$$

Perturbation Theory:

$$\begin{cases} \delta(\vec{k},t) = \sum_n a^n(t)\,\delta_n(\vec{k}) \\ \theta(\vec{k},t) = \mathcal{H}(t)\sum_n a^n(t)\,\theta_n(\vec{k}) \end{cases} \qquad (\Omega = 1)$$

nth order solution

$$\delta_n(\vec{k}) = \int d^3q_1 \ldots d^3q_n\, \delta_D(\vec{k}-\vec{q}_1-\ldots-\vec{q}_n)\, F_n^{(s)}(\vec{q}_1,\ldots,\vec{q}_n)\,\delta_1(\vec{q}_1)\cdots\delta_1(\vec{q}_n)$$

➡ Solve recursively for F_n

Peebles, Fry, Goroff, et al. Juszkiewicz, et al. Jain Bertschinger

Skewness + Bias in N-body Simulations

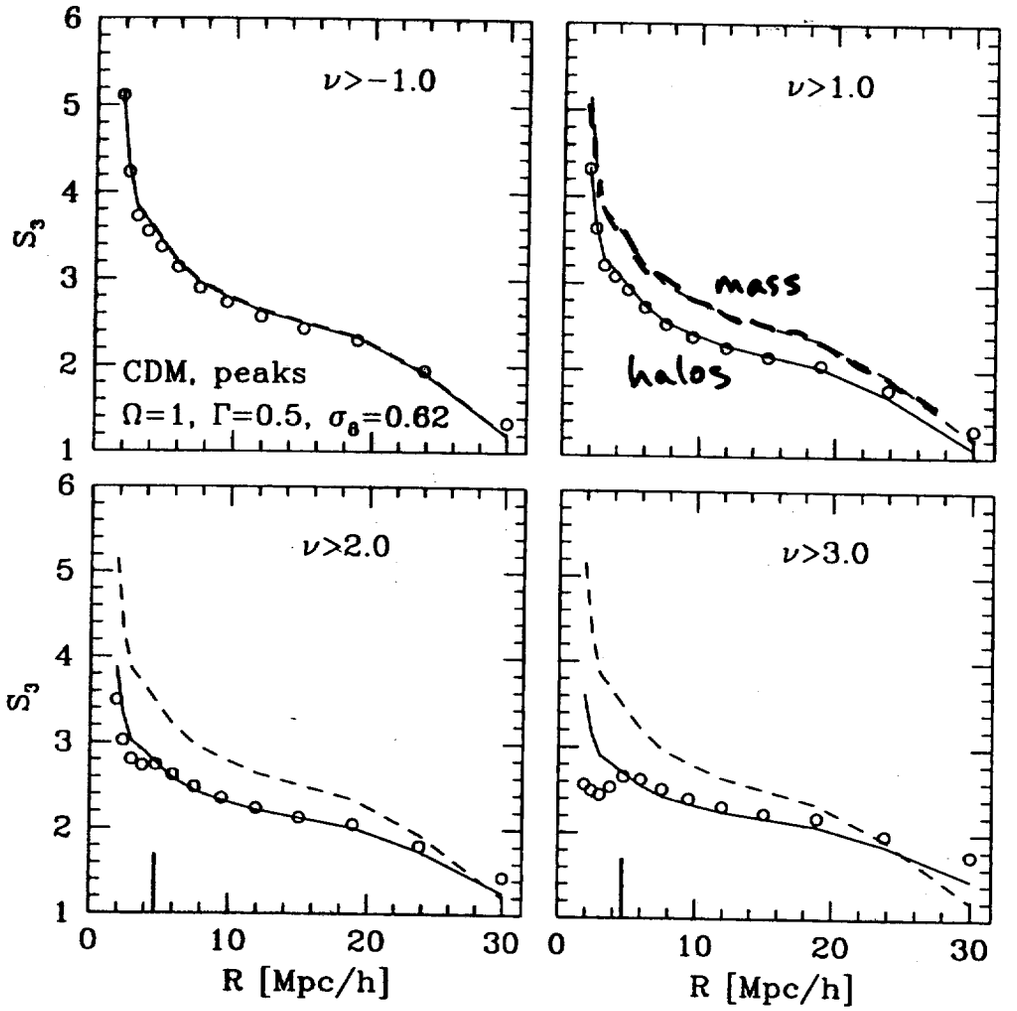

Fig. 1a.— The skewness of density peaks with different heights ν predicted by our model (solid curves) compared with that derived from N-body simulations (circles). The dashed curves show the skewness of the mass density distribution in the simulation. Results are shown for the standard cold dark matter model with $(\Omega, \Gamma, \sigma_8) = (1.0.5, 0.62)$. The thick ticks on the horizontal axis show the values of R where $\bar{\xi}_2(R) = 1$.

Jing, Mo, White

Probing Bias with Higher Order Moments

Local bias: $\delta_{gal}(\vec{x}) = f(\delta(\vec{x})) = \sum_{k=1}^{\infty} \frac{b_k}{k!} \delta^k$

(i.e., probability of forming luminous galaxy only depends on local density field)

Higher Moments Sensitive to Non-linear Bias:

- Fry + Gaztañaga
- Juszkiewicz, Bouchet, Weinberg, Amsterdamski, Chodorowski

$$S_3^{(gal)} = \frac{1}{b_1}\left[S_3^{(matter)} + \frac{3b_2}{b_1}\right] + \dots$$

(b_1: linear bias; $\frac{3b_2}{b_1}$: non-linear bias)

$$S_4^{(gal)} = \frac{1}{b_1^2}\left[S_4^{(m)} + 12\frac{b_2}{b_1}S_3^{(m)} + 4\frac{b_3}{b_1} + 12\frac{b_2^2}{b_1^2}\right] + \dots$$

$$S_J^{(gal)} = \frac{1}{b_1^{J-2}} S_J^{(m)} + \dots$$

Non-local bias: $\delta_{gal}(\vec{x}) = F\left[\int_V \delta(\vec{x}')\, W(\vec{x}'-\vec{x})\, d^3x'\right]$

Breaks the scaling hierarchy: $W(r)$ introduces characteristic scale

Scale-dependent bias: $P_g(\vec{k}) = b(k)\, P_p(\vec{k})$

N.B.: Bias likely stochastic as well.

APM Moments vs. Perturbation Theory

Gaztañaga, " + JF

$S_J = \bar{\xi}_J / \bar{\xi}_2^{J-1}$

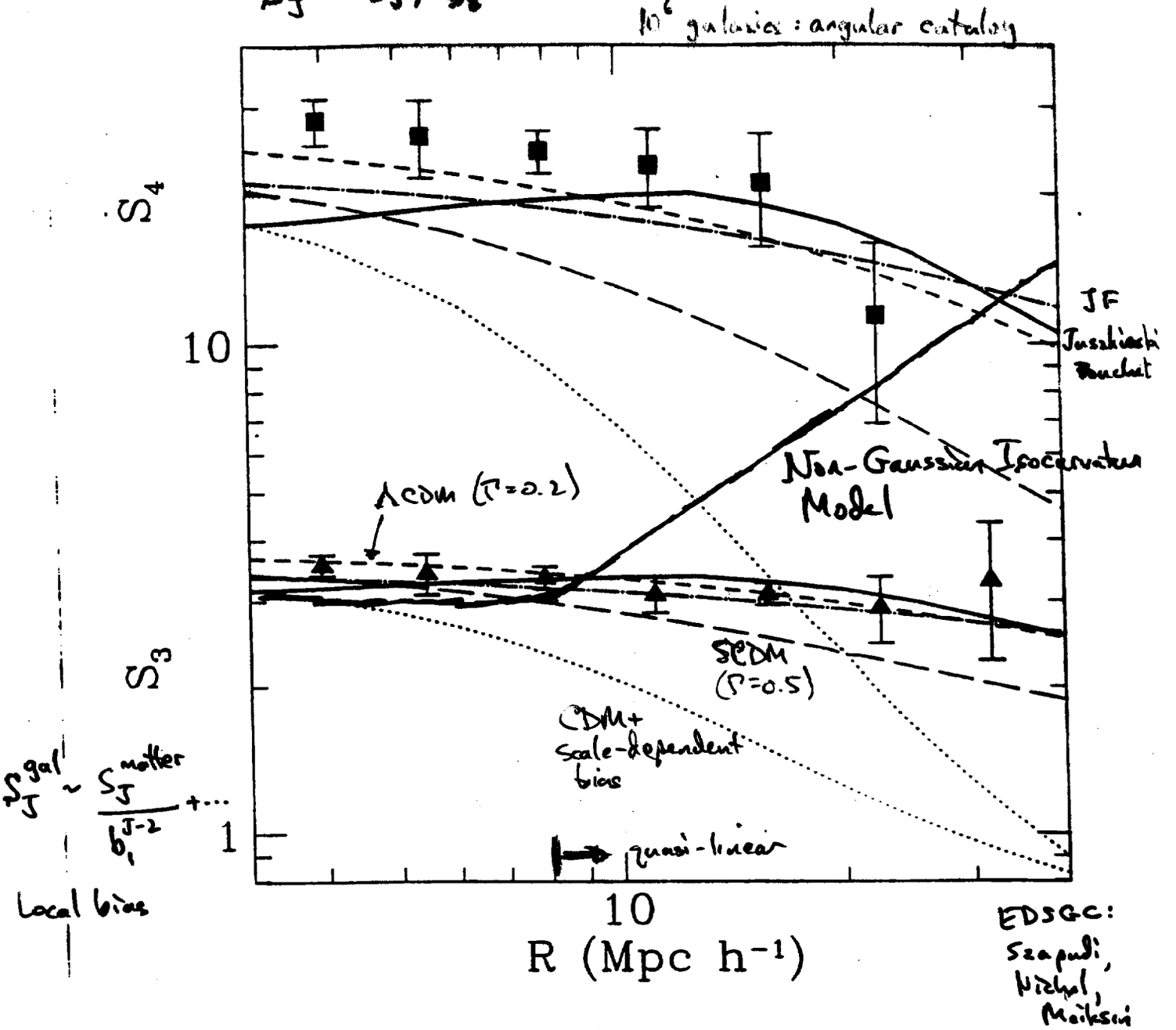

Assumptions here: $b_1 = 1$, $b_{J>1} = 0$, Gaussian I.C.

Simplest interpretation: APM galaxies trace mass on large scales + consistent with NL evolution from Gaussian. I.C.

Gaussian vs. Non-Gaussian Initial Conditions

Gaussian:

- simple
- motivated by simplest inflation models

$$\frac{\delta\rho}{\rho} \propto \delta\varphi_{inf}$$

Free, massless field in de Sitter vacuum state ≃ Gaussian

- agrees with S_J observations

Non-Gaussian:

- interesting
- motivated by topological defects and some inflation models:

$$\rho(\vec{x}) \propto \varphi_{in}^2(\vec{x})$$

- Lyth
- Muller + Schmid
- Matsuda, et al.
- Linde + Mukhanov
- Peebles: Isocurvature CDM model

- non-Gaussian tails for early structure formation
- constrained by S_J observations: broken scaling

Goztañaga + Makonen Fry + Scherrer Jing, Jing, Börner, Borgani

- Liddle + Mukherjee
- Antoniadis, et al.
- Peebles

Non-Gaussian Inflation Models

- Isocurvature Perturbations with "Blue" $n_s > 1$ Spectra

- Non-Gaussian Initial Distribution

"Gaussian-Squared" Models

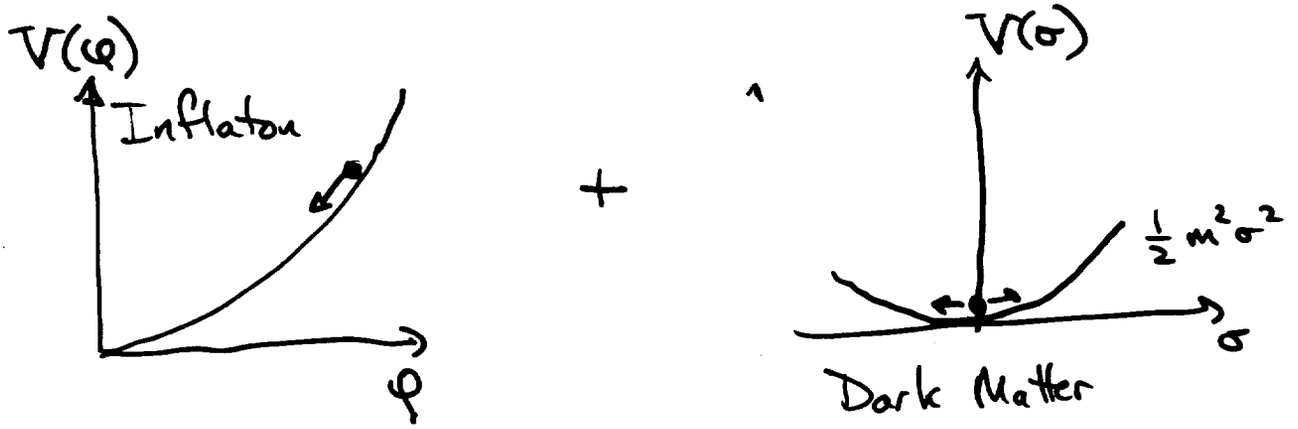

Density Perturbation: φ, σ Gaussian random fields

$$\delta(\vec{x}) \triangleq \frac{V_\sigma(\vec{x}) - \langle V_\sigma \rangle}{\langle V_\sigma \rangle} = \frac{\sigma^2(\vec{x})}{\langle \sigma^2 \rangle} - 1$$

Two-Point Correlations:

$$\xi_\rho(x_{12}) = \langle \delta(\vec{x}_1)\,\delta(\vec{x}_2) \rangle = 2\frac{\langle \sigma(\vec{x}_1)\,\sigma(\vec{x}_2) \rangle^2}{\langle \sigma^2 \rangle^2}$$

Three-Point Fn:

$$\xi_{123} = \langle \delta_1 \delta_2 \delta_3 \rangle = 2\sqrt{2}\left(\xi_\rho(\vec{x}_{12})\xi_\rho(\vec{x}_{23})\xi_\rho(\vec{x}_{31})\right)^{1/2}$$